Location of Deuterium Positions in the Proton-Conducting Perovskite BaCe$_{0.4}$Zr$_{0.4}$Sc$_{0.2}$O$_{2.90}$·xD$_2$O by Neutron Powder Diffraction

Abul K. Azad and John T. S. Irvine*

School of Chemistry, University of St. Andrews, Fife KY16 9ST, Scotland, United Kingdom

Received April 28, 2008

Structural studies from X-ray and high-resolution neutron powder diffraction data collected on deuterated and nondeuterated BaCe$_{0.4}$Zr$_{0.4}$Sc$_{0.2}$O$_{2.9}$·x(D$_2$O) have been carried out. Although X-ray diffraction suggested that a sample of the nominal composition was single phase cubic, neutron diffraction showed the structure as single phase orthorhombic in the space group *Pbnm*. The structural distortion can be related to the determination of accurate oxygen positions in the structure by neutron diffraction. Rietveld refinement of the neutron diffraction data and subsequent Fourier nuclear density maps have proved to be successful in locating the deuterium (D) positions despite the low occupancies present, with a final composition of BaCe$_{0.4}$Zr$_{0.4}$Sc$_{0.2}$O$_{2.90}$·0.10(D$_2$O) and the D position associated with the O1 position in the Ba-containing plane. TGA analysis in dry air on the deuterated sample shows the 0.70% weight loss for heating from room temperature to 900 °C which corresponds to the D$_2$O loss of 0.10/formula unit. The unit-cell volume for the deuterated phase was found to be higher than the nondeuterated phase (i.e., dry) at 295 K, i.e., $V = 311.59(5)$ Å^3 compared with 310.91(5) Å^3. The O1–D distance was found to be 1.06(1) Å. The presence of anisotropic displacements for oxygen was observed during the refinement.

1. Introduction

Solid oxide fuel cells (SOFCs) are attracting considerable interest as the next-generation energy conversion devices because of their high efficiency and low emissions. Proton-conducting solid electrolytes with high and pure protonic conductivity have a wide range of technological applications in fuel cells, batteries, sensors, hydrogenation/dehydrogenation of hydrocarbons, electrolyzers, etc.[1-3] Presently, the most favored oxide ion conducting electrolyte is yttria-stabilized zirconia (YSZ) with operating temperature in the range 800–1000 °C. Although there are some advantages to high-temperature operation, such high temperatures do present a number of problems as well, such as degradation, sealing, and materials selection. Therefore, new materials showing high conductivity at lower temperatures are required, and in this respect, proton conducting solid electrolytes are promising in the development of intermediate temperature solid oxide fuel cells (IT-SOFCs).[4,5]

Perovskite-type oxide materials (general formula, ABO$_3$) are mainly studied as proton conducting electrolytes for the target operating temperature in the range 400–700 °C. Acceptor doped alkaline earth cerates and zirconates have been thoroughly studied because of the great interest in their possible applications as solid proton conductors.[6-9] Barium cerates, e.g. BaCe$_{0.9}$Y$_{0.1}$O$_{3-\delta}$, generally exhibit the highest proton conductivities; however, these materials are unstable at high temperature in the presence of CO$_2$ and steam.[6,7] On the other hand, alkaline earth zirconates such as calcium, strontium, or barium zirconates show, in general, better chemical and mechanical stability than the analogous cerates, but lower protonic conductivity. When trivalent cations are doped on the B-site, some of the zirconates show pure protonic conductivity in hydrogen atmosphere at high temperature (600–1000 °C).[9,10] The n-type conductivity was found to be relatively high under reducing conditions in barium cerate and other cerates, whereas it is almost negligible in the zirconates.[2] A solid proton conductor that combines the high chemical stability of the zirconates and the high conductivity of the cerates is very interesting to study.[11,12] Perovskites with Ba at the A site and trivalent cation substitution with cerium and zirconium at the B site is now an important area of extensive investigation because of its high durability and good protonic conductivity.[13-17]

* Corresponding author. Tel: 44 1334 463817. Fax: 44 1334 463808. E-mail: jtsi@st-andrews.ac.uk.

(1) Iwahara, H. *Solid State Ionics* **1995**, *77*, 289.
(2) Norby, T. *Solid State Ionics* **1999**, *125*, 1.
(3) Colomban, Ph., Ed. *Proton Conductors: Solids, Membranes and Gels-Materials and Devices*; Cambridge University Press, Cambridge, U.K., 1992.
(4) Iwahara, H.; Matsumoto, H.; Takeuchi, K. *Solid State Ionics* **1999**, *125*, 285.
(5) Kreuer, K. D. *Ann. Rev. Mater. Res.* **2003**, *33*, 333.
(6) Chen, F. L.; Sorensen, O. T.; Meng, G. Y.; Peng, D. K. *J. Mater. Chem.* **1997**, *7*, 481.
(7) Bhide, S. V.; Virkar, A. V. *J. Electrochem. Soc.* **1999**, *146*, 2038.
(8) Iwahara, H.; Uchida, H.; Tanaka, S. *Solid State Ionics* **1983**, *9–10*, 1021.
(9) Bohn, H. G.; Schober, T. *J. Am. Ceram. Soc.* **2000**, *83*, 768.
(10) Iwahara, H.; Tajima, T.; Hibino, T.; Ozaki, K.; Susuki, H. *Solid State Ionics* **1993**, *61*, 65.
(11) Laidoudi, M.; Abu Talib, I.; Omar, R. *J. Phys. D: Appl. Phys.* **2002**, *35*, 397.
(12) Tao, S.; Irvine, J. T. S. *Adv. Mater.* **2006**, *18*, 1581.
(13) Savaniu, C. D.; Canalez-Vazquez, J.; Irvine, J. T. S. *J. Mater. Chem.* **2005**, *15*, 598.
(14) Katahira, K.; Kohchi, Y.; Shimura, T.; Iwahara, H. *Solid State Ionics* **2000**, *138*, 91.

Moreover, doping of Sc at the B site has been found to be beneficial in improving conductivity and stability of the structure,[18] hence the choice of the composition $BaCe_{0.4}Zr_{0.4}Sc_{0.2}O_{2.90}$ in this study. The acceptor doped perovskites possess oxygen vacancies which allow proton incorporation via the dissociation of water as shown in the following equation

$$H_2O(g) + O_O^x + V_O^{\cdot\cdot}O \leftrightarrow 2(OH)_O^{\cdot} \qquad (1)$$
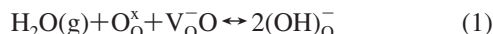
Proton conduction occurs by the hopping of a proton from one oxygen to the next. By locating these protons within the material, a conduction mechanism can be hypothesized. Despite the considerable interest, relatively few articles have been published in which proton positions have been successfully defined from experiments. An earlier neutron diffraction study by Knight located a potential proton position in $BaCeO_3$ and $BaCe_{0.9}Y_{0.1}O_{2.95}\cdot xH_2O$, associated with the bridging oxygens.[19,20] Ito et al.[21] have investigated the proton position in $BaSn_{0.5}In_{0.5}O_{2.75}$, a heavily doped system. In cubic systems, protons have been found at or very close to the 12h site in the $Pm\bar{3}m$ space group, which was supported by the modeling studies of $BaCeO_3$ and $(Ca/Ba)ZrO_3$.[21-24] The results of these studies are consistent with respect to the hydrogen site; a hydrogen atom bound to an oxygen atom with an O–H distance approximately 1 Å, and the O–H is directed roughly along the bisector of the two edges of the two adjacent BO_6 octahedra. A schematic diagram of proton incorporation in a cubic perovskite structure has been given in Figure 1. Similar position and interatomic distances were also observed in orthorhombic structures theoretically[25] and experimentally.[19,26] Sata et al.[27] have reported the proton position in D_2O and H_2O-dissolved lightly Sc-doped $SrTiO_3$ single crystals by neutron diffraction. They conclude that hydrogen atoms occupy a site between two oxygen atoms of BO_6 octahedron with a separation of 1.2 Å and an O–H direction leaning slightly toward B site ions. Ahmed et al.[28] have observed the deuterium position at the 24k Wyckoff positions of the $Pm\bar{3}m$ space group in $BaZr_{0.5}In_{0.5}O_{3-y}$.

In this study, neutron powder diffraction (NPD) measurements were carried out in order to investigate the structure and determine the proton sites. NPD is the most direct method to characterize crystal structure including light
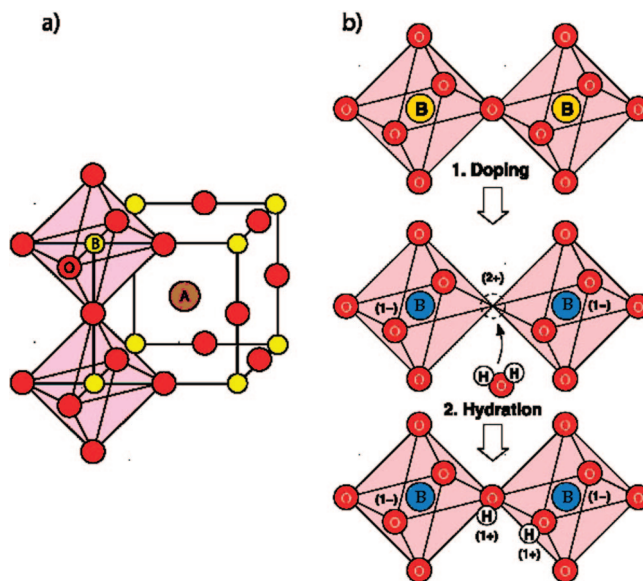

Figure 1. Schematic diagram of proton incorporation in a perovskite structure. (a) Simple perovskite, (b) B-site doping and proton incorporation (A cation has not shown for simplicity).

elements. Because of the large incoherent scattering cross-section of protons to thermal neutrons, it has generally been necessary to fully deuterate samples. The positive scattering cross-section of deuterium ($b = 6.671$ fm) also allows for an independent check on any position determined for hydrogen atom ($b = -3.739$ fm).[29] We have selected the nominal composition $BaCe_{0.4}Zr_{0.4}Sc_{0.2}O_{3-\delta}$, which contains a high number of oxygen vacancies allowing for an increased degree of proton incorporation when heated in wet atmospheres, thereby potentially allowing for the reliable identification of the proton sites. Our previous conductivity measurements showed significant proton conduction between 300 and 450 °C (3.3×10^{-4} S cm^{-1} at 400 °C in wet 5% H_2/Ar) for this material, with X-ray diffraction structural studies suggesting a cubic structure.[18] We have collected neutron diffraction data on deuterated and nondeuterated $BaCe_{0.4}Zr_{0.4}Sc_{0.2}O_{2.90}$ in order to identify the proton position in the structure. NPD data have been collected at very low temperature (5 K) to high temperature (500 K) on deuterated sample. Low-temperature data is very important to freeze out lattice vibration, reduce the Debye–Waller factor, and probably reduce the number of accessible alternative sites available to the protons at higher temperature. We have used the combined approach of Rietveld refinement and Fourier nuclear density map to locate the protons in the structure.
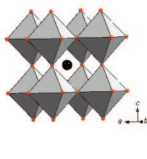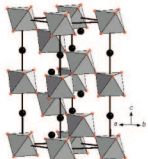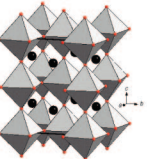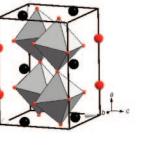
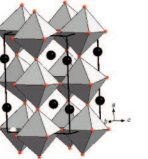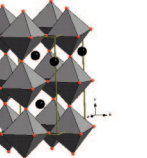## 2. Experimental Section

Polycrystalline samples of $BaCe_{0.4}Zr_{0.4}Sc_{0.2}O_{3-\delta}$ (BCZS20) were prepared by solid state reaction of $BaCO_3$, CeO_2, ZrO_2 and Sc_2O_3 powders. The sample preparation has been described in detail elsewhere.[18] After final sintering, pellets showed a density corresponding to ~70% of the theoretical value. Phase purity, identity and homogeneity were confirmed by X-ray powder diffraction (XRD) using a STOE Stadi P transmission diffractometer (Cu Kα_1 = 1.5406Å) and an EDX Inca Energy System.

(15) Ryu, K. H.; Haile, S. M. *Solid State Ionics* **1999**, *125*, 355.
(16) Taniguchi, N.; Nishimura, C.; Kato, J. *Solid State Ionics* **2001**, *145*, 349.
(17) Shimada, T.; Wen, C.; Taniguchi, N.; Otomo, T.; Takahashi, H. *J. Power Sources* **2004**, *131*, 289.
(18) Azad, A. K.; Irvine, J. T. S. *Solid State Ionics* **2007**, *178*, 635.
(19) Knight, K. *Solid State Ionics* **2001**, *145*, 275.
(20) Knight, K. *Solid State Ionics* **2000**, *127*, 43.
(21) Ito, T.; Nagasaki, T.; Iwasaki, K.; Yoshino, M.; Matsui, T.; Igawa, N.; Ishii, Y. *Solid State Ionics* **2007**, *178*, 13.
(22) Glöckner, R.; Islam, M. S.; Norby, T. *Solid State Ionics* **1999**, *122*, 285.
(23) Davis, R. A.; Islam, M. S.; Gale, J. D. *Solid State Ionics* **1999**, *126*, 323.
(24) Islam, M. S.; Davis, R. A.; Gale, J. D. *Chem. Mater.* **2001**, *13*, 2049.
(25) Shi, C.; Morinaga, M. *J. Comput. Chem.* **2006**, *27*, 711.
(26) Kendrick, E.; Knight, K. S.; Islam, M. S.; Slater, P. R. *Solid State Ionics* **2007**, *178*, 943.
(27) Sata, N.; Hiramotom, K.; Ishigame, M.; Hosoya, S.; Niimura, N.; Shin, S. *Phys. Rev. B* **1996**, *54*, 15795.
(28) Ahmed, I.; Knee, C. S.; Karlsson, M.; Eriksson, S.-G.; Henry, P. F.; Matic, A.; Engberg, D.; Börjesson, L. *J. Alloys Compd.* **2008**, *450*, 103.

(29) Sears, V. F. *Neutron News* **1992**, *3*, 26.

Deuterium Positions in BaCe$_{0.4}$Zr$_{0.4}$Sc$_{0.2}$O$_{2.90}$·xD$_2$O

Chem. Mater., Vol. 21, No. 2, 2009 217

Table 1. Comparison of Tilt Systems and R-Factors Using Different Space Groups for the Rietveld Refinement of BaCe$_{0.4}$Zr$_{0.4}$Sc$_{0.2}$O$_{3-\delta}$ at Room Temperature (295 K)

Space group	*Pm-3m*	*R-3c*	*I4/mcm*	*Imma*	*Pmcn*	*Pbnm*
Glazer's Tilt system	$a^0a^0a^0$	$a^-a^-a^-$	$a^0a^0c^-$	$a^0b^-b^-$	$a^+b^-b^-$	$a^-b^+a^-$
R-factors						
R$_p$ (%)	7.63	6.93	5.88	6.32	5.40	4.64
R$_{wp}$ (%)	12.40	8.83	7.69	8.04	6.85	5.96
R$_{exp}$ (%)	4.50	4.51	4.50	4.51	4.51	4.51
R$_B$ (%)	17.02	9.70	6.59	8.51	6.11	5.82
R$_F$ (%)	10.37	6.07	3.65	5.65	4.29	4.55
χ^2	7.53	3.83	2.90	3.18	2.31	1.75
3D view						

The phase-pure samples were placed in an alumina crucible and placed inside a tube furnace. The sample was heated at 1250 °C for 6 h in air then cooled down to 275 °C under an Ar gas flow bubbled through D$_2$O for 48 h. Thermogravimetric analysis was carried out on deuterated material on a NETZSCH TG 209 with TASC 414/3 controller from 25 to 900 °C (5 °C/min) under flowing air at a rate of 35 mL/min.

NPD data were collected on the D2B diffractometer at the Institut Laue-Langevin (ILL), Grenoble, France. A neutron wavelength of $\lambda = 1.5937$ Å was used. The step scan covered a 2θ range 0−158.6° with a step size of 0.05°. A vanadium can was used as the sample holder. Only room temperature data were collected for the dried sample. The sample was dried in a furnace at 900 °C and kept in a sealed glass bottle until putting in to a vanadium can for NPD. For the deuterated sample data were collected at three different temperatures, e.g., 5, 300, and 500 K. All data sets were analyzed by the Rietveld method using the FullProf software.[30] The diffraction peak shapes were described by a pseudo-Voigt function and the background intensities were described by Chebyshev polynomial with six coefficients. Peak asymmetry corrections were made during the refinements.

3. Results and Analysis

3.1. Structure of Nondeuterated BaCe$_{0.4}$Zr$_{0.4}$Sc$_{0.2}$O$_{3-\delta}$. Indexing and preliminary Rietveld refinement of the X-ray diffraction data suggested the sample as single phase cubic in the *Pm$\bar{3}$m* space group.[18] However, the neutron diffraction pattern showed some extra low intensity peaks (e.g., $d =$ 2.5822, 1.9637, 1.4437, 1.3017, 1.1961 Å), which could not

be indexed in the cubic symmetry. The space groups *R$\bar{3}$c*, *Pmcn*, *Imma*, *I4/mcm*, and *Pbnm* (*cab* setting of *Pnma*) were considered. Of these space groups, the orthorhombic *Pbnm* space group showed the correct peak reflections and gave the best Rietveld refinement fit with reasonable *R*-factors and structural parameters. A comparison of tilt systems, 3D structures and *R*-factors obtained using different space groups is presented in Table 1. The lattice parameters of the orthorhombic perovskite with space group *Pbnm* (Z = 4) are derived from the cubic prototype cell (*Pm$\bar{3}$m*, Z = 1) as $a \approx \sqrt{2}a_0$, $b \approx \sqrt{2}a_0$, and $c \approx 2a_0$ ($a_0 \approx 3.89$ Å). For *Pbnm*, the cell parameters were found to be $a > b$, which is consistent with previous studies on barium cerate, where it was also pointed that two different metrics were possible in this space group (independent of setting) depending upon whether the length of the unit-cell edge associated with the glide operation direction is the smallest or second smallest edge.[19,31] Figure 2 shows the Rietveld refinement of the NPD data at room temperature for the nondeuterated sample. Many perovskite structures are distorted, and orthorhombic perovskites are not uncommon e.g. orthorhombic distortion was observed in Y^{3+}- and Nd^{3+}-doped BaCeO$_3$ from high-resolution neutron powder diffraction.[19,31] The occupancies of the two oxygen sites were initially allowed to vary and the vacancies appeared to be associated with the O1 position. The overall oxygen content was found to be O$_{2.94(2)}$, which is larger than the expected value 2.90 to conserve charge

(30) Rodriguez-Carvajal, J. *Physica B* **1993**, *192*, 55.

(31) Kruth, A.; Mather, G. C.; Jurado, J. R.; Irvine, J. T. S. *Solid State Ionics* **2005**, *176*, 703.
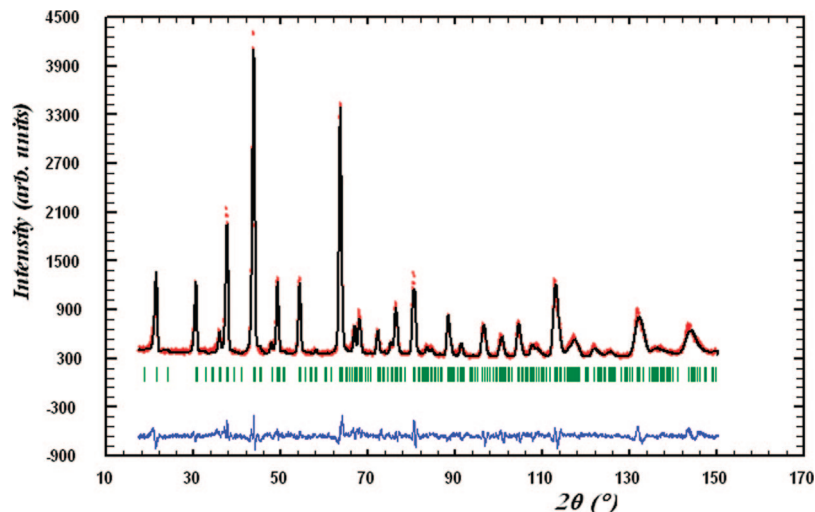
Figure 2. Rietveld refinement profile of the neutron powder diffraction data of nondeuterated $BaCe_{0.4}Zr_{0.4}Sc_{0.2}O_{2.90}$ collected at room temperature. Observed data, calculated pattern, and the difference profile are shown as points, solid line and continuous line below, respectively. The tick marks show the position of Bragg reflections predicted by the structural model.

Table 2. Summary of Results Obtained from Rietveld Analysis of Neutron Powder Diffraction Data for Non-Deuterated and Deuterated $BaCe_{0.4}Zr_{0.4}Sc_{0.2}O_{2.90}$ at Different Temperatures in the Orthorhombic Symmetry (space group *Pbnm*, $Z = 2$)

params	nondeuterated		deuterated		
	300 K	5 K	5 K	300 K	500 K
structure model	without D position	without D position	with D position	with D position	with D position
a	6.0482(5)	6.0413(5)	6.0418(5)	6.0520(5)	6.0640(5)
b	6.0059(6)	6.0015(5)	6.0029(6)	6.0117(6)	6.0230(6)
c	8.5595(8)	8.5447(8)	8.5485(8)	8.5639(8)	8.5819(7)
V (Å³)	310.91(5)	309.80(5)	310.04(5)	311.59(5)	313.44(5)
Ba 4c (x, y, 0.25)					
x	0.011(1)	0.012(1)	0.009(2)	0.005(4)	0.006(3)
y	0.0222(7)	0.019(1)	0.0181(9)	0.017(1)	0.017(2)
B (Å²)	0.82(6)	0.50(2)	0.49(9)	1.09(9)	1.44(9)
Ce/Zr/Sc 4b (0.5, 0, 0)					
B (Å²)	1.21(6)	0.91(4)	0.87(5)	1.06(5)	1.26(5)
O1 4c (x, y, 0.25)					
x	−0.0465(9)	−0.052(9)	−0.0504(8)	−0.043(1)	−0.036(1)
y	0.503(1)	0.503(1)	0.503(2)	0.503(2)	0.501(2)
B (Å²)	1.60(7)	0.95(4)	0.5(1)	1.45(9)	1.08(5)
O2 8d (x, y, z)					
x	0.757(1)	0.758(2)	0.757(1)	0.759(1)	0.758(1)
y	0.258(1)	0.242(1)	0.244(1)	0.243(2)	0.243(1)
z	−0.0139(6)	−0.0162(8)	−0.0196(6)	−0.0144(9)	−0.0153(9)
B (Å²)	1.89(5)	1.30(7)	1.25(8)	1.24(7)	1.18(8)
overall oxygen occupancy: (O1+O2)/3	0.98(2)	1.00(2)	1.00	1.00	1.00
D 4c (x,y,0.25)					
x			0.4316(2)	0.4316(1)	0.4316(1)
y			0.1325(9)	0.1325(1)	0.1325(1)
B (Å²)			6.4(6)	8.5(6)	8.9(9)
$D_{occup/f.u.}$			0.200(2)	0.200(2)	0.200(2)
R_p	4.64	5.89	5.54	5.20	4.96
R_{wp}	5.96	7.57	7.09	6.68	6.35
R_B	5.82	9.53	6.90	7.05	7.09
R_F	4.55	8.11	6.65	7.44	8.39
χ^2	1.75	2.11	1.87	1.66	1.54

neutrality. So, some of the oxygen positions were filled because of autoprotonation of the material. The occupancies of cations were also checked and confirmed to the targeted stoichiometries within standard deviation. Detailed structural information and *R*-factors from the refinements are summarized in Table 2 and selected bond distances are listed in Table 3. It is noticeable from the refined structural parameters that the thermal parameters for the oxygen positions are high. Similarly high thermal parameters have been reported for cubic/pseudocubic variants of oxygen deficient perov-

skites.[27,32,33] The obtained *Pbnm* space group is due to the local structural distortions related to the displacements of oxygen positions. In addition, the high values may also be partly related to the differing ionic radii of Ce^{4+} (ionic radius 0.87 Å) and Zr^{4+} (ionic radius 0.72 Å) partially substituted

(32) Berastegui, P.; Hull, S.; Garcia-Garcia, F. J.; Eriksson, S.-G. *J. Solid State Chem.* **2002**, *164*, 119.
(33) Becerro, A. I.; Redfern, S. A. T.; Carpenter, M. A.; Knight, K. S.; Seifert, F. *J. Solid State Chem.* **2002**, *167*, 459.

Deuterium Positions in BaCe₀.₄Zr₀.₄Sc₀.₂O₂.₉₀·xD₂O

Chem. Mater., Vol. 21, No. 2, 2009 219

Table 3. Main Bond Distances (≤3.5 Å) and Octahedral Distortion for Non-Deuterated and Deuterated BaCe₀.₄Zr₀.₄Sc₀.₁O₂.₉₀ Determined from NPD Data

	nondeuterated		deuterated	
	295 K	5 K	300 K	500 K
Ce/Zr/Sc—O₆ Octahedra				
B^a—O1 (Å) (× 2)	2.1584(8)	2.158(1)	2.156(1)	2.157(6)
B—O2 (Å) (× 2)	2.198(8)	2.14(1)	2.15(1)	2.15 (1)
B—O2 (Å) (× 2)	2.070(8)	2.13 (1)	2.13 (1)	2.13 (1)
V_{BO6} (Å³)	13.0731	13.1237	13.1407	13.1776
⟨Mn—O⟩ (Å)	2.142(8)	2.143(1)	2.145(6)	2.146(6)
distortion^b (Δ)	0.0597	0.0131	0.0121	0.0126
D—O1 (Å) (× 2)		1.06(1)	1.03(1)	1.02(1)
D—B (Å) (× 2)		2.3175(2)	2.3216(2)	2.3264(2)
D—O2 (Å) (× 2)		3.102(2)	3.099(7)	3.091(8)
D—O2 (Å) (× 2)		2.356(8)	2.370(7)	2.392(8)
D—Ba (Å)		2.65(1)	2.67(1)	2.67(1)
D—Ba (Å)		2.34(6)	2.344 (6)	2.35(1)
Ba—O₁₂ Polyhedra				
Ba—O1 (Å)	3.135(9)	3.12(1)	3.11(1)	3.12(1)
Ba—O1 (Å)	2.912(9)	2.93(1)	2.93(1)	2.93(1)
Ba—O1 (Å)	2.813(9)	2.77(1)	2.80(1)	2.85(2)
Ba—O1 (Å)	3.239(9)	3.252(9)	3.25(1)	3.22(2)
Ba—O2 (Å) (× 2)	3.079(8)	3.07(9)	3.06(1)	3.05(1)
Ba—O2 (Å) (× 2)	2.833(8)	2.86(1)	2.89(1)	2.91(1)
Ba—O2 (Å) (× 2)	2.981(8)	2.89(1)	2.91(1)	2.93(1)
Ba—O2 (Å) (× 2)	3.201(8)	3.261(9)	3.24(1)	3.24(1)

^{a} B = B-site cations Ce, Zr, and Sc. ^{b} Distortion (Δ) = (longest bond length − shortest bond length)/average bond length.
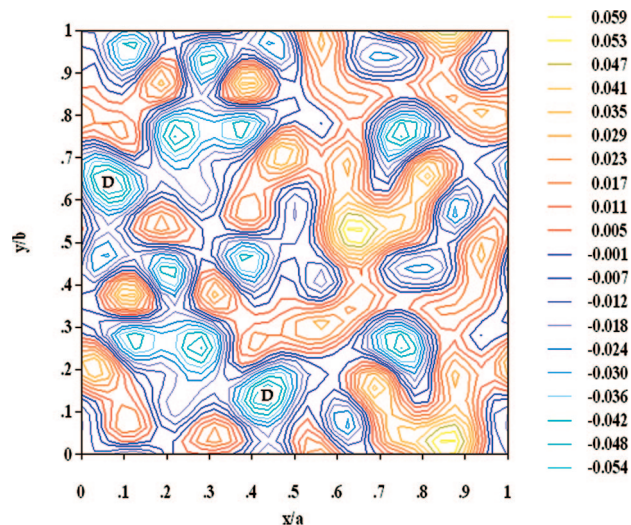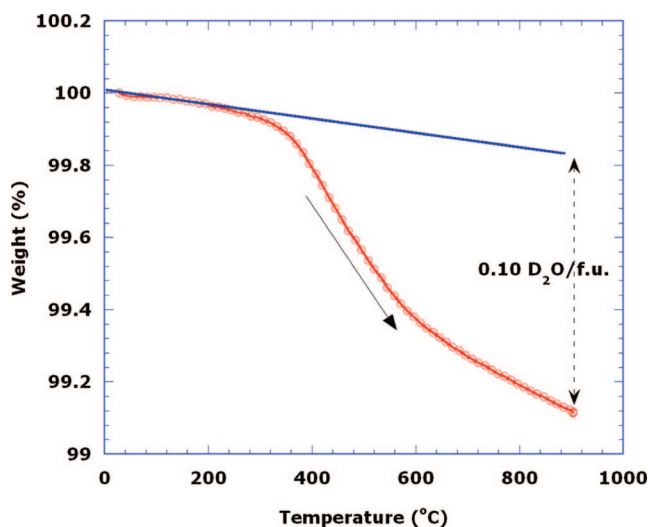
Table 4. Anisotropic Thermal Parameters for O1 and O2

name	$U_{11} \times 100$ (Å²)	$U_{22} \times 100$ (Å²)	$U_{33} \times 100$ (Å²)
295 K			
O1	0.48(4)	1.54(3)	0.41(4)
O2	0.39(5)	0.58(6)	0.50(3)
5 K			
O1	1.01(2)	1.69(2)	0.35(6)
O2	0.21(4)	0.07(1)	0.60(7)
300 K			
O1	0.95(8)	1.53(5)	0.68(6)
O2	0.18(4)	0.26(1)	0.84(7)
500 K			
O1	1.00(1)	1.67(1)	0.62(4)
O2	0.09(8)	0.14(3)	0.73(6)

Figure 3. Fourier nuclear density maps obtained from neutron diffraction data of the *ab* plane at $z = 0.25$ show missing scattering density attributed to D.

Figure 4. TGA plot of deuterated BaCe₀.₄Zr₀.₄Sc₀.₂O₂.₉₀ sample heated in dry air at 5 °C/minut up to 900 °C.

by Sc³⁺ (ionic radius 0.745 Å).[34] In agreement with this interpretation is the observed anisotropy in the oxygen thermal parameters (Table 4).

3.2. Structure of Deuterated BaCe₀.₄Zr₀.₄Sc₀.₂O₂.₉₀₊δ. Neutron diffraction data were collected for the deuterated sample at 5, 300, and 500 K. All patterns showed the material with the *Pbnm* space group in which the extra, noncubic peaks, confirming orthorhombic symmetry, were more apparent. In the refinement of the D₂O/Ar heated samples, the cation occupancies were fixed at the values observed for the nondeuterated sample at room temperature. Refinement of low-temperature (5 K) data converged with comparatively high R-factors (R_p = 5.89%, R_{wp} = 7.57%, R_B = 9.53%) and χ^2 = 2.11, indicating the incomplete nature of the structural model. The oxygen site occupancy in this phase was estimated to be complete within the detection level of Rietveld analyses.

To locate the missing nuclear density, we calculated Fourier nuclear density maps. Inspection of density maps in

the *ab*-plane at $z = 0.25$ (Figure 3a), a strong positive peak at (0.4316, 0.1325, 0.25) consistent with the positive scattering length of 6.671 fm of deuterium. This site is located close to the oxygen O1 (−0.0502, 0.5026, 0.25) and gives a chemically sensible O−D distance of 1.06 Å at 5 K The O1 site corresponds to the 4c Wyckoff site in *Pbnm* symmetry, and D was therefore introduced close to this position. The refinement converged yielding improved R-factors and goodness-of-fit (see Table 2). The site occupancy and the isotropic/anisotropic atomic displacement parameter of deuterium atom were optimized in the calculation while composition constraint was imposed according to the equation

$$D_2O + V_O^{\bullet\bullet} \rightarrow 2D^\bullet + O_O^x \tag{2}$$

Thermogravimetric analysis (TGA) measurements were performed to determine the D₂O content in the structure. TGA analysis on deuterated samples in air shows a mass loss of 0.70% occurs during heating from room temperature to 900 °C, which corresponds to the loss of 0.10 D₂O per
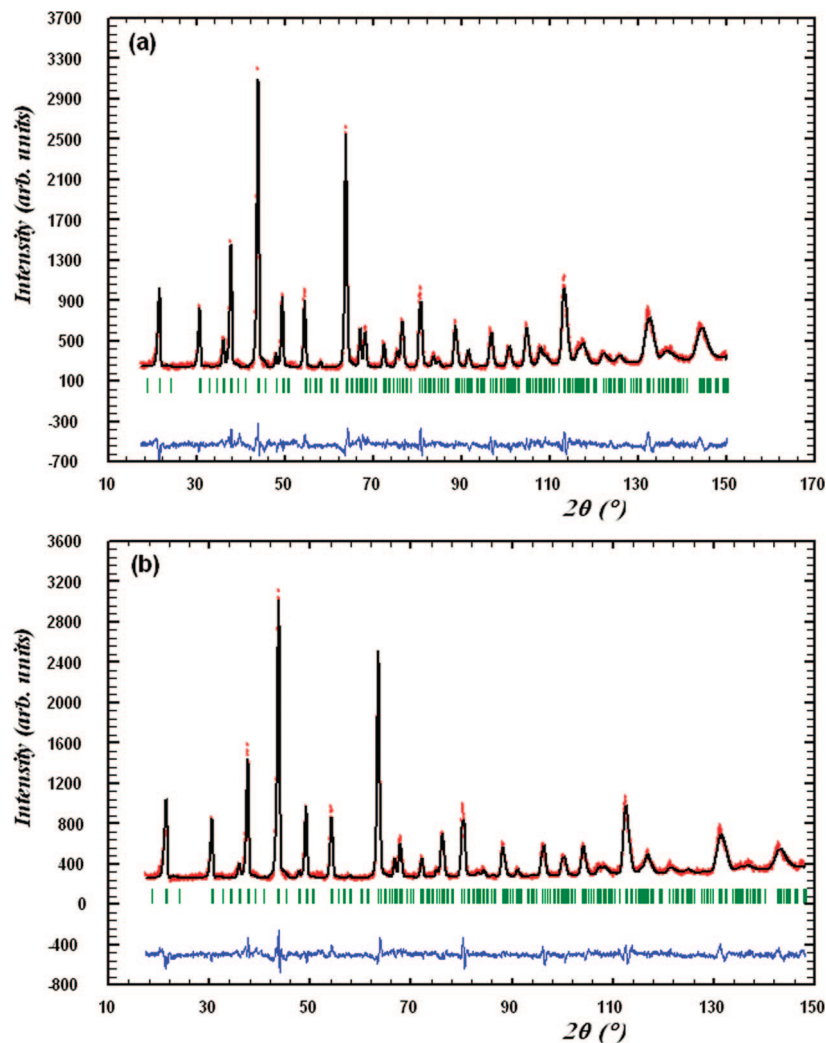
(34) Shannon, R. D. *Acta Crystallogr., Sect. A* **1976**, *32*, 751.

Figure 5. Rietveld refinement profile of the neutron powder diffraction data of $BaCe_{0.4}Zr_{0.4}Sc_{0.2}O_{2.90} \times 0.10(D_2O)$ collected at (a) 5 and (b) 500 K. Observed data, calculated pattern, and the difference profile are shown as points, solid line, and continuous line below, respectively.

formula unit. Figure 4 shows the TGA plot of the deuterated sample in dry air. Considering the oxygen vacancies to be occupied by D_2O, a composition of $BaCe_{0.4}Zr_{0.4}Sc_{0.2}O_{2.90} \times 0.10(D_2O)$ can be obtained, which is similar to the composition obtained from neutron diffraction data refinement.

The D_2O occupancy was then fixed to be 0.10 in the Rietveld refinement of the NPD data, which converged in to reasonably good R-factors and confirm the chemical formula as $BaCe_{0.4}Zr_{0.4}Sc_{0.2}O_{2.90} \times 0.10(D_2O)$. According to this formula, no oxygen positions were vacant after the deuteration process. During the deuteration reaction (eq 2) it was believed that each oxide vacancy was filled by an OD group while the remaining dissociated D^+ ion became attached to a nearby oxygen ion. Panels a and b in Figure 5 show the Rietveld refinement profile of the deuterated samples at 5K and 500K. Figure 6 shows the schematic 3D representation of $BaCe_{0.4}Zr_{0.4}Sc_{0.2}O_{2.90} \times 0.10(D_2O)$ with D in the $4c$ position.

The refinement of NPD data collected at 300 and 500 K on deuterated samples was performed using the model for 5 K keeping the same profile parameters and cation fractional occupancies. The thermal displacement parameters were a little larger and the cell volumes were expanded. The cell parameters were increased because of the thermal vibration of the atoms keeping the same orthorhombic symmetry. The refinements converged into good R-factors. A small decrease in O1−D distance was observed with increasing temperature.

4. Discussion

Utilizing neutron diffraction measurements at different temperatures, a detailed structural study of the perovskite proton conducting oxide of nominal starting composition $BaCe_{0.4}Zr_{0.4}Sc_{0.2}O_{2.90}$ has been performed. Although the X-ray diffraction patterns suggested a single-phase cubic material,[18] analyses of neutron diffraction data showed a single phase orthorhombic structure. Infrared spectroscopy and first principle calculation by Karlsson et al.[35] on proton conducting $BaIn_xZr_{1-x}O_{3-x/2}$ shows that, even in the pure cubic system, the local structure is distorted. Ahmed et al.[28] have observed the deuteron position on a 12 h (0.5,0.217,0) crystallographic site in cubic $BaZr_{0.5}In_{0.5}O_{2.5}$-$(OD)_{0.5}$ (space group $Pm\bar{3}m$) with O−D distance of 0.92(2) Å. They also propose the deuterium site as $24k$ with anisotropic displacement of oxygen positions and observed

(35) Kalsson, M.; Björketun, M. E.; Sundell, P. G.; Matic, A.; Wahnström, G.; Engberg, D.; Börjesson, L.; Ahmed, I.; Eriksson, S.; Berastegui, P. *Phys. Rev. B* **2005**, *72*, 094303.
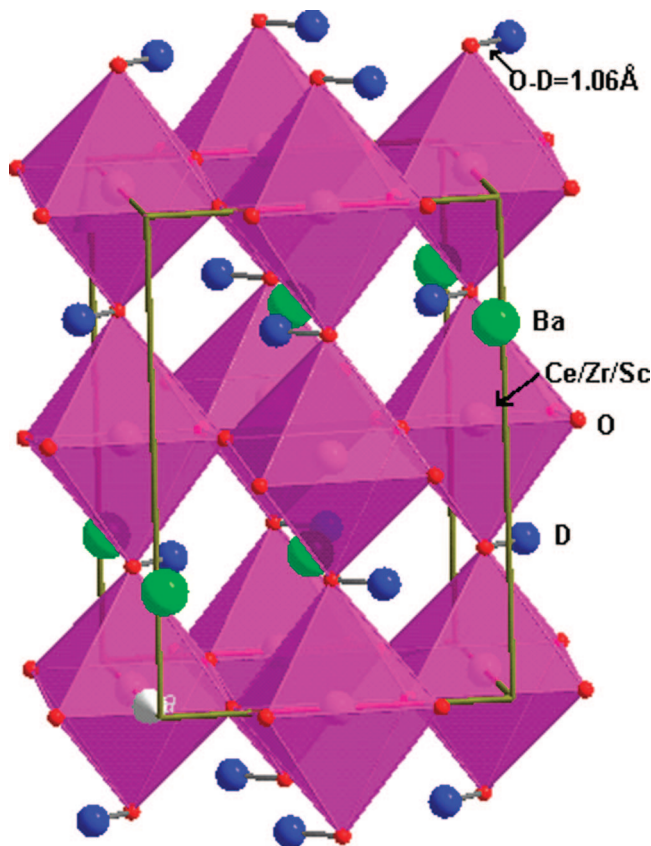
Deuterium Positions in BaCe$_{0.4}$Zr$_{0.4}$Sc$_{0.2}$O$_{2.90}$·xD$_2$O

Chem. Mater., Vol. 21, No. 2, 2009 221

Figure 6. Schematic three-dimensional diagram of BaCe$_{0.4}$Zr$_{0.4}$Sc$_{0.2}$O$_3$.D$_{0.20}$.

Figure 7. (a) Representation of the refined 4c structural site for the deuteron in BaCe$_{0.4}$Zr$_{0.4}$Sc$_{0.2}$O$_{2.90}$ × 0.10(D$_2$O) at 5 K. (b) Anisotropic atomic displacement parameters of the oxygen ions.

a short-range deviations from cubic symmetry by Raman spectroscopy for both dried and hydrated samples. Knight[20] has suggested the proton position associated with the O2 at 8d (0.13,0.77,0.34) crystallographic site in BaCe$_{0.9}$Y$_{0.1}$O$_{2.95}$ in the orthorhombic space group *Pmcn*. This was the only site that behaved in a stable manner and converged to a chemically reasonable bond length of 0.93 Å. Kendrick et al.[26] have found the proton position associated with the O1 at 4c (0.494,0.25,0.027) crystallographic site in La$_{0.73}$Ba$_{0.27}$ScO$_{2.865}$.0.135(H/D)$_2$O in the orthorhombic space group *Pnma* with O1−D distance is 0.94(2) Å. In this study, we have observed the deuteron position associated with O1 at 4c (−0.05,0.503,0.25) in the orthorhombic space group *Pbnm* having O1−D distance is 1.06(1) Å. No indication of Ba evaporation or second phase was observed. TGA and Rietveld refinement of neutron data showed this material to have the composition BaCe$_{0.4}$Zr$_{0.4}$Sc$_{0.2}$O$_{2.90}$ × 0.10(D$_2$O).

The unit-cell volume and the BO$_6$ octahedral volume in deuterated sample is larger than for the nondeuterated sample at room temperature (295 K), as observed in previous studies on other proton conducting systems, e.g. doped BaCeO$_3$.[36] The cell parameter expansion can be correlated to an expansion of the Ce/Zr/Sc−O bond distances, which may be related to the presence of protons, leading to a reduction in the average charge of the oxide ion site. Another key factor to explain the increased B−O bond distances is the increase in the average B site coordination number as the oxide ion vacancies are filled. In addition, to the B−O bond length
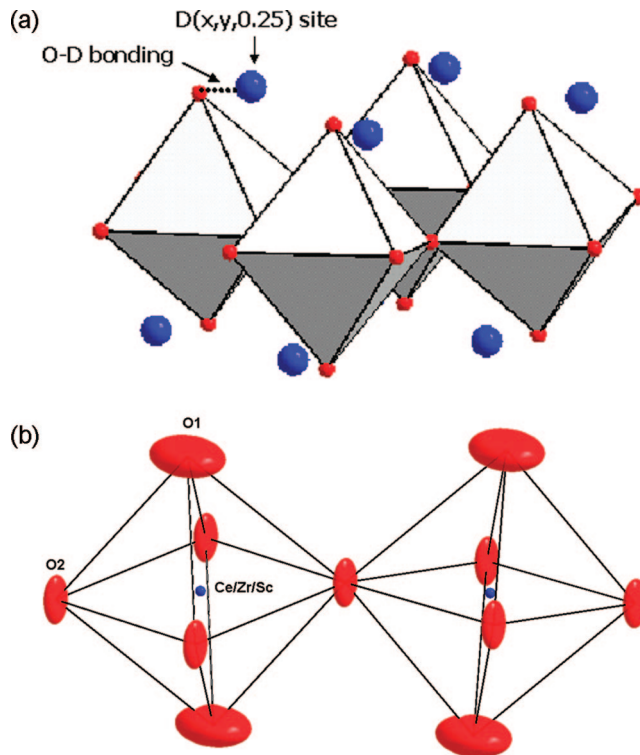
changes, there are also considerable changes to the Ba−O distances, with a shortening of 8 of the bonds and a lengthening of the remaining 4. Utilizing difference Fourier nuclear density analysis of the neutron diffraction data it was possible to identify the proton site. The proton is associated with the oxygen (O1), in the *ab* plane leaning toward B site cations. The O1-D distance was found to decrease with increasing temperature. From the refined D position, it is difficult to conclude about the possibility of O2−D bonds because the shortest distance is about 2.35 Å. The proton migration mechanism is likely to involve proton transfer between the O1 and O2 site (Grötthus mechanism), and may be aided by lattice vibrational distortions shortening the O2−D distance, similar to results predicted from modeling studies on proton conducting CaZrO$_3$.[24] The idealized deuterium position was associated with the O1 in the *ab*-plane (Figure 7a) which is similar to the site described in refs 25 and 26.

The evidence of oxygen disorder has implications for the calculated O−D distances obtained for the deuterated phase. The structural refinements performed for both the nondeuterated and deuterated phases revealed that the oxygen sites strongly favor anisotropic atomic displacement parameters. The most likely explanation for this is static and localized displacement of O ions. In this respect, similarly anisotropic thermal parameters have been reported for cubic/pseudocubic variants of oxygen deficient perovskites.[26,28] The anisotropic displacement at the O1 position (parallel to the *ab*-plane) was higher than the O2 position (parallel to the *bc* or *ac*-plane) (Figure 7b). The evidence of oxygen disorder has implications for the O−D distances obtained for the deuterated phase. The rotations and/or tilts of the BO$_6$ octahedra,

(36) Yamaguchi, S.; Yamada, N. *Solid State Ionics* **2003**, *162−163*, 23.

implicit from the anisotropic oxygen displacement components, can be expected to influence proton transport.

The local oxygen displacements may be responsible for the reduction in the symmetry to orthorhombic as we have found in our system. In these distorted systems, oxygen-to-oxygen separations between connecting octahedra are significantly reduced, facilitating interoctahedra proton transfer.[37] The small deviations from cubic symmetry can play an important role for proton hopping as oxygen vibrations are believed to be intimately linked to proton transfer in perovskite oxides.[38] As mentioned in the introduction, Ito et al. have found the protons at the bisector $12h$ site in the cubic $Pm\bar{3}m$ space group with the O−D distance of ~1.0 Å. On the other hand, Sata et al. found the hydrogen atoms in the "hydrogen-bond site" between two oxide ions of a BO_6 octahedron, with O−H leaning slightly toward B cations with an O−H distance about 1.2 Å in $SrTi_{1-x}Sc_xO_{3-x/2}$ ($x = 0.02$ and 0.03).[26] In the present study, we have found the deuterium atoms to occupy a chemically similar position between two BO_6 octahedra and O1-D bond was slightly leaning toward B cations with an O1−D distance of about 1.06 Å.

(37) Islam, M. S. *J. Mater. Chem.* **2000**, *10*, 1027.
(38) Münch, W.; Seifert, G.; Kreuer, K. D.; Maier, J. *Solid Sate Ionics* **1996**, *66−68*, 647.

5. Conclusions

By using a standard solid-state synthesis route, it was possible to obtain single-phase $BaCe_{0.4}Zr_{0.4}Sc_{0.2}O_{3-\delta}$ samples. Rietveld analysis of the NPD data indicates that the samples crystallize in orthorhombic symmetry. An expansion in the unit-cell volume and BO_6 octahedra was observed because of the proton association and increase of temperature. TGA measurements show that the D_2O uptake is about 0.10/f.u. at room temperature. The proton site in the proton conducting system $BaCe_{0.4}Zr_{0.4}Sc_{0.2}O_{2.90} \times 0.10(D_2O)$ has been located through application of a Rietveld refinement of the NPD data and subsequent Fourier electron density map calculation. The protons are associated with the O1 ($4c$ Wykoff site) in the ab-plane, in the site between B−O−B ions which consist in the edge of an oxygen octahedron. The shortest O1−D distance was found to be 1.06(1) Å at 5 K.